Research Article | Vol. 10, No. 8 | 1 Aug 2019 | BIOMEDICAL OPTICS EXPRESS 3899
Biomedical Optics EXPRESS

Systematic study of the effect of ultrasound gel on the performances of time-domain diffuse optics and diffuse correlation spectroscopy

LAURA DI SIENO,[1,*] DAVIDE CONTINI,[1] GIUSEPPE LO PRESTI,[2] LORENZO CORTESE,[2] TONY MATEO,[3] BOGDAN ROSINSKI,[3] ELENA VENTURINI,[4] PIETRO PANIZZA,[4] MIREIA MORA,[5] GLORIA ARANDA,[5] MATTIA SQUARCIA,[5] ANDREA FARINA,[6] TURGUT DURDURAN,[2,7] PAOLA TARONI,[1,6] ANTONIO PIFFERI,[1,6] ALBERTO DALLA MORA[1]

[1]*Politecnico di Milano - Dipartimento di Fisica, Milano, Italy*
[2]*ICFO - Institut de Ciències Fotòniques, The Barcelona Institute of Science and Technology, Castelldefels (Barcelona), Spain*
[3]*VERMON S.A., Tours, France*
[4]*Scientific Institute (IRCCS) Ospedale San Raffaele - Breast Imaging Unit, Milano, Italy*
[5]*IDIBAPS, Fundació Clínic per la Recerca Biomèdica, Barcelona, Spain*
[6]*Consiglio Nazionale delle Ricerche - Istituto di Fotonica e Nanotecnologie, Milano, Italy*
[7]*Institució Catalana de Recerca i Estudis Avançats (ICREA), Barcelona, Spain*
**laura.disieno@polimi.it*

Abstract: Recently, multimodal imaging has gained an increasing interest in medical applications thanks to the inherent combination of strengths of the different techniques. For example, diffuse optics is used to probe both the composition and the microstructure of highly diffusive media down to a depth of few centimeters, but its spatial resolution is intrinsically low. On the other hand, ultrasound imaging exhibits the higher spatial resolution of morphological imaging, but without providing solid constitutional information. Thus, the combination of diffuse optical imaging and ultrasound may improve the effectiveness of medical examinations, e.g. for screening or diagnosis of tumors. However, the presence of an ultrasound coupling gel between probe and tissue can impair diffuse optical measurements like diffuse optical spectroscopy and diffuse correlation spectroscopy, since it may provide a direct path for photons between source and detector. A systematic study on the effect of different ultrasound coupling fluids was performed on tissue-mimicking phantoms, confirming that a water-clear gel can produce detrimental effects on optical measurements when recovering absorption/reduced scattering coefficients from time-domain spectroscopy acquisitions as well as particle Brownian diffusion coefficient from diffuse correlation spectroscopy ones. On the other hand, we show the suitability for optical measurements of other types of diffusive fluids, also compatible with ultrasound imaging.

1. Introduction

The worldwide growing research efforts and funding for multimodal imaging diagnostic devices highlight their importance as they permit to overcome limitations of the different single measurement techniques by combining their strengths, enabling in particular the acquisition of complementary morphological, compositional and/or functional information to maximize the diagnostic potential of a single examination [1]. Common techniques involved in this process include computed tomography, positron emission tomography, single-photon emission computed tomography and magnetic resonance imaging [2–7]. However, other solutions are being investigated to combine cheaper and safer (label-free, non-ionizing and

#365978 https://doi.org/10.1364/BOE.10.003899
Journal © 2019 Received 24 Apr 2019; revised 1 Jul 2019; accepted 1 Jul 2019; published 11 Jul 2019

Biomedical Optics EXPRESS

non-invasive) alternative techniques. Among those, diffuse optical techniques exploit the propagation of visible and near-infrared light inside biological tissues to obtain functional and constitutional information [8]. Diffuse optical spectroscopy (DOS), for instance, allows the assessment of absorption and reduced scattering coefficients of tissues. Thus, when performed at different wavelengths, functional parameters related to blood and tissue composition can be estimated from the absorption spectrum, while the scattering spectrum provides information about the microstructure like the density and size of biological cells and subcellular components [9]. Another complementary optical technique is diffuse correlation spectroscopy (DCS), which allows the estimation of the microvascular blood flow by measuring the speckle fluctuations of coherent light backscattered by biological tissues [10]. This can be useful in many clinical contexts related to neurology (e.g. to assess the cerebral blood flow) and oncology (e.g. to characterize microvascular blood flow in tumors). Both techniques can probe tissues down to a depth of few centimeters, but they suffer from limited spatial resolution due to the diffusive nature of tissues [11]. For this reason, the combination of optical techniques with any other technique capable of providing morphological information, like ultrasound (US) [12–18] or magnetic resonance [19–25] imaging, is considered a promising solution to improve the effectiveness of medical examinations.

Diffuse optical techniques are well known to be prone to artifacts due to the motion of the probe holding both light injection and collection optical fibers (or alternatively holding directly the light source and the detector) or due to a not effective contact between probe and tissue [26,27]. In particular, both DOS and DCS measurements can be severely affected by a possible propagation of light in the air gap between probe and tissue under investigation. As the light injected and traveling inside the tissue is attenuated by different orders of magnitude before being re-emitted at the collection position, even a small fraction of light propagating directly from source to detector (i.e. not passing through tissue) can have detrimental effects on the measurement [28,29]. Hence, the combination of US imaging and optical techniques is particularly unlucky as an acoustically impedance-coupling fluid between probe and tissue is needed to improve the transmission of the US wave, but it can offer an undesired direct path for light from the injection to the detection point.

This work has a double aim: i) to report a systematic investigation on the effect of direct light propagation on both DOS and DCS measurements using a standard water-clear US coupling gel; ii) to identify alternative fluids with suitable optical and ultrasound properties (in particular as will be shown some scattering contribution) preventing direct light leakage.

2. Materials and methods

2.1 Tested fluids

In this work we tested 5 different fluids (see Fig. 1) serving as an interface between probe and phantom. More in detail, we considered two commercially-available US gels: a water-clear one (Cogel Ultrasound, Comedical s.r.l., Italy) and a turbid one (Polysonic Ultrasound Lotion, Parker Laboratories Inc., USA). We also tested the water-clear US gel after addition of a home-made 1% w/w dispersion of TiO_2 particles to make it turbid. Finally, we used two commercially-available body lotions: one with high viscosity (labeled hereinafter “Body lotion 1”, Cutimed® Protect, BSN Medical GmbH, Germany) and one with low viscosity (labeled hereinafter “Body lotion 2”, Tena Skin Lotion, Tena S.p.A., Italy).

Biomedical Optics EXPRESS

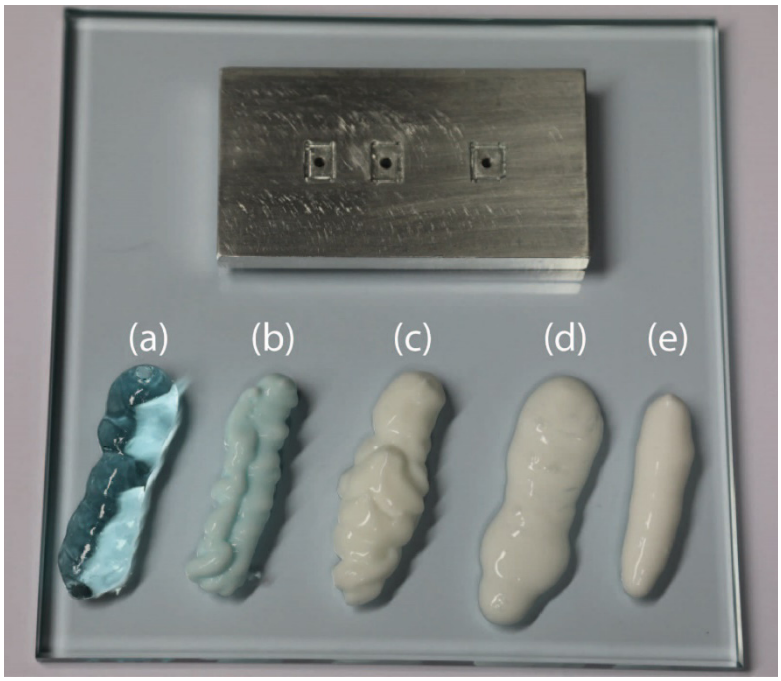

Fig. 1. Top: probe used for the measurements. Bottom: fluids used as contact interface between probe and sample where (a) is a commercially-available water-clear gel; (b) is a water-clear gel with TiO_2 addition; (c) is a commercially-available turbid US gel; (d) and (e) are body lotions with low and high viscosity respectively (body lotion 2 and 1, respectively).

2.2 DOS measurements

Setup

The DOS measurements were carried on using a state-of-the-art time domain broadband diffuse optical spectroscopy system [30]. It is based on a supercontinuum source (Fianium Whitelase S360, NKT Photonics, Denmark), which provides picosecond optical pulses (at 60 MHz repetition rate). The wavelength selection was performed by means of a rotating prism whose movement was software-controlled. The monochromatic light was then injected into a 50 µm-core fiber and then sent to a fiber-to-fiber u-bench holding a stack of variable optical attenuators to tune the amount of light injected in the sample. Finally, from the output of the u-bench, photons were sent to the sample through a 100 µm-core fiber. Using an optical switch, two different points were sequentially illuminated, permitting measurements at two distinct source-detector distances (SDD). The re-emitted photons were collected using a 1-mm-core optical fiber set at 2 cm and 3 cm distance from the 2 source fibers, respectively. Then a doublet lens imaged with unit magnification the fiber tip onto the detector (a 1 mm^2 area SiPM, for further details see [31]). The recording of the distribution of times-of-flight (DTOF) was achieved using a Time-Correlated Single-Photon Counting board (SPC130, Becker&Hickl GmbH, Germany). Both injection and collection fibers were hosted into holes in an aluminum probe (see Fig. 1). The fibers were not touching directly the sample, but were in contact with a small glass window (0.55 mm thick gorilla glass), which was glued inside a recess in the aluminum plate to avoid any fluid accumulation under the fibers' tips, thus avoiding possible artifacts during the measurement. Separate glasses (each one covering a single fiber tip) were fixed inside different recesses in the aluminum plate, not protruding from it and actually resulting in a flat probe surface. The use of separate glasses was chosen to prevent direct paths between source and detector fibers. It is worth noting that this solution was preferred with respect to the direct contact between fibers and phantom under

Biomedical Optics EXPRESS

investigation also because the direct contact of the fiber tip is not possible in a real combined optical-ultrasound probe for medical imaging, due to the need to avoid the presence of small gaps where bacteria can proliferate and to the need for the probe to be waterproof for adequate cleaning. A possible alternative for covering the fiber tips is to consider a thin film of Mylar or an absorbing thin film like a gelatin or acetate cut-off filter (e.g., Kodak Wratten filters). The former interface has already been validated in diffuse optics [32] as it provides the sufficient amount of scattering to break possible direct light propagation between source and detector. The latter can prevent direct light propagation thanks to its absorption coefficient. These solutions are preferable when a unique window has to be used to cover all the fiber tips, but its use on real optical-ultrasound probes is prevented by their fragility. Additionally, even if direct light propagation in the Mylar film or Wratten filter is not possible, the light short circuit can still occur, as a matching fluid between film (or filter) and tissue under investigation is required to couple the ultrasound signal with the tissue.

Measurements and data analysis

As previously stated, the presence of direct light can distort the DTOF shape thus severely impairing DOS measurements and leading to an erroneous retrieval of the optical properties (absorption – μ_a – and reduced scattering – μ_s' – coefficients) of the medium under analysis. To prove the suitability of the fluids, we performed measurements over a wide range of optical properties. To this extent, we acquired μ_a and μ_s' spectra from a set of homogeneous solid phantoms based on epoxy resin with calibrated quantities of black toner and TiO_2 powder to tune the absorption and reduced scattering coefficient, respectively [33]. Those phantoms are part of a phantom kit proposed more than 10 years ago for the implementation of the MEDPHOT protocol for the characterization of diffuse optical instruments [33]. The MEDPHOT protocol aims in particular at evaluating the performance of diffuse optical systems in recovering optical properties of homogeneous highly scattering media. As the phantoms are part of a growing effort of standardization of performance assessment procedures in the field of diffuse optics, they have been measured many times in the past with standard black optical probes, without matching fluids or glass windows. Hence, many reference measurements can be found in the literature (see for instance [30,33–39]). Here we used 16 phantoms (out of the 32 phantoms composing the MEDPHOT kit), featuring all possible combinations of 4 μ_a values (nominal values at 800 nm: 0.05, 0.15, 0.25 and 0.35 cm^{-1}) and 4 μ_s' values (nominal values at 800 nm: 5, 10, 15 and 20 cm^{-1}). For each phantom, measurements were acquired in 6 conditions. Firstly, we used all the 5 fluids (one at the time) between the reflective metal probe and the phantom surface. In each case, few milliliters of fluid were spread on the phantom surface. Then, the probe was pressed on the phantom to reach the contact between the probe and the phantom, squeezing out most of the fluid, leaving under the probe just a residual thin layer. Due to the limited thickness of the fluid layer, the possible presence of absorption peaks in the fluid (e.g., at 980 nm for water-based gels) is not expected to give any significant effect on the recovery of the optical properties of the phantom as it can only result into a signal intensity attenuation, while using the time-domain diffuse optical technique the information is provided by the signal shape. After cleaning both phantom and probe, for comparison purpose, we used a thin adhesive black velvet tape interface (thickness of about 300 μm) glued to the probe surface without any fluid in between (yielding what we consider as a reference measurement). The tape had three windows of the same size as the glass windows (around 11 x 10 mm^2), thus not hiding possible effects of the glass on the measurement. This interface is often used for standard DOS measurements, as it prevents direct light propagation.

For each phantom and in each condition, DTOFs in the range from 600 to 1100 nm (in steps of 10 nm) were acquired and, for each wavelength, 5 repeated measurements of 1 s each were recorded. With the same acquisition scheme also the Instrument Response Functions (IRFs) were saved. As dictated by the BIP protocol [40], to acquire the IRF injection and

Biomedical Optics EXPRESS

collection fibers were faced using a stable holder and, a thin layer of Teflon was inserted in between to fill all the propagation modes in the collection fiber, thus adequately duplicating the conditions of phantom measurements. In all cases, the target count-rate was about 500 kcps.

To retrieve the optical properties of each phantom, the recorded DTOFs were fitted to the analytical model of a semi-infinite diffusive medium obtained under the diffusion approximation [41]. The fitting range was set from 50% of the peak on the rising edge to 1% on the falling edge of each DTOF. To improve the robustness of the fitting procedure, the 5 repetitions were summed and the background subtracted. Non-idealities of the system were taken into account convolving the analytical model to the experimental IRF.

In order to quantitatively assess the discrepancy in the retrieval of optical properties when using a coupling fluid with respect to the reference measurement (i.e., using the black velvet to prevent light channeling), we compute the relative percentage error ($\varepsilon_{\%}$) as:

$$\varepsilon_{\%} = \frac{\mu^{(fluid)} - \mu^{(reference)}}{\mu^{(reference)}} * 100$$

where μ can be either the absorption or the reduced scattering coefficient.

2.3 DCS measurements

Setup

The DCS measurements were performed using a custom DCS device built at ICFO. The DCS device source consists of a single longitudinal mode continuous wave laser (iBeam smart 785, Toptica, Germany) emitting at 785 nm. Light was injected in the phantom through a multimode fiber (200 μm core) and the diffused reflectance was acquired through two fiber bundle consisting of 4 single mode fiber each. The detection part is characterized by 8 single-photon avalanche diodes (SPCM-AQ4C, Excelitas, Canada). The intensity temporal autocorrelation function g_2 of each channel was calculated by an 8-channel digital correlator (correlator.com – USA). Source and detection fiber bundle tips were placed at a distance of 2 and 3 cm in reflectance geometry, using the very same probe as used for the DOS experiment and described above.

The liquid phantom for the DCS experiment consists of an emulsion of lipid droplets (Lipofundin 20%, B. Braun Melsungen AG, Germany) in water. The concentration of Lipofundin 20% in water was chosen in order to obtain a reduced scattering coefficient of 10 cm^{-1}, and water absorption, as described in ref [42]. The reduced scattering coefficient of the phantom was then verified through DOS measurements. The liquid phantom was placed in a black plastic phantom box. The frontal wall of the container has a transparent Mylar window (whose use in diffuse optics has been validated in Ref [32]) of approximately the same dimension as the fiber holder, thus allowing the injection of laser light into the liquid and the collection of the diffused signal.

Measurements and data analysis

The acquired intensity temporal autocorrelation functions g_2 were transformed into electric field temporal autocorrelation functions g_1, which were fitted with the solution of the correlation diffusion equation for a semi-infinite medium, in order to retrieve the particle Brownian diffusion coefficient (D_b) [10]. In the DCS fitting routine the absorption and reduced scattering coefficients of the liquid phantom were kept fixed in all cases (μ_a = 0.026 cm^{-1} and μ_s' = 10 cm^{-1}). The fluids and black velvet tape were used with the same procedures described for DOS measurements. In each case, 20 repetitions of the DCS acquisitions were recorded in order to compute mean and standard deviation of the recovered D_b.

Biomedical Optics EXPRESS

2.4 Ultrasound imaging experiment

Ultrasonic imaging experiment was carried out on a quality assessment US phantom (Gammex 404GS LE with 0.5 dB/cm/MHz attenuation from Sun Nuclear Corporation) using a Verasonics L22-14v high-frequency linear array, having an 18-MHz center frequency, 75% relative bandwidth (~80 µm wavelength) and an elevation focal length of 18 mm. The probe was driven by a 256 channels Vantage (Verasonics, Inc., Kirkland, WA), which is an ultrasound open platform intended for research. The imaging mode used is Plane Wave Compounding consisting of a transmit of 31 plane waves (unfocused) tilted from −15° to 15° (1° angular resolution) followed by a synthetic beamforming of all radiofrequency data (on all channels) acquired during each transmit to achieve the image reconstruction process. Imaging process was based on the speed of sound (SoS) in the US phantom (1540 m/s), which correspond to the average SoS in human soft tissues. Transmitted pulse consisted of one cycle at 15.625 MHz with 30 V peak amplitude. Same settings are used in both transmit and receive for all acquisitions.

The goal of the experiment is to assess the ability of all studied coupling fluids to ensure proper acoustic coupling for ultrasonic imaging. Main required qualities for a good acoustic coupling are low attenuation that keep optimal depth of penetration and SoS matching with the explored medium (the same if possible) to reach best possible spatial resolution and also avoid spatial distortions. Following the same approach used for DOS and DCS measurements, where the potential detrimental effect of the fluids on optical measurements was maximized by using a highly reflective probe, the US imaging experiment was designed to emphasize the potential detrimental effects of the coupling fluids in order to identify the best coupling agent. Thus, the US probe was moved away from the phantom interface and was tilted by about 18° to both have enough coupling fluid thickness (till 5 mm) that emphasizes attenuation, and have significant varying coupling agent thickness to emphasize artifacts stemming from SoS mismatching. The use of a high frequency probe provides also more sensitivity to phase aberration stemming from the coupling agent in case of SoS mismatching with the explored medium.

Two regions of the phantom were imaged. First one is made of two cysts of different diameter (4 and 8 mm) to appreciate contrast resolution and geometric fidelity. Second one consists of few thin wires to appreciate spatial resolution and geometric fidelity also. The regions of interest are in both cases located between 15 to 20 mm depth.

3. Results and discussions

3.1 DOS measurements

Figure 2 (Fig. 3) and Fig. 4 (Fig. 5) report the graphs of the absorption and reduced scattering spectra obtained on the 16 phantoms at 2 cm (3 cm) source-detector distance using all coupling fluids as well as the black velvet (standard condition). More in detail, for each row (fixed μ_s') the spectra for 4 phantoms with increasing μ_a (columns) are reported. In each graph, colors encode the different fluids used as well as the standard condition.

The absorption spectra (see Fig. 2 and Fig. 3) clearly demonstrate a huge deviation of the μ_a recovered when using the water-clear gel with respect to the standard condition (black lines in all the graphs). In particular, for phantoms with higher scattering (rows) and higher absorption (columns) the measured μ_a is highly underestimated. It has to be noted that for a given phantom the discrepancy between the value of absorption recovered (i.e. given panel in Fig. 2 and Fig. 3) with the water-clear gel and the other fluids is not constant. For example, in Fig. 2, the phantoms reported in the last two columns (i.e. with higher absorption) clearly show that for shorter wavelengths (e.g. 600 nm), the absorption coefficient recovered when using the water-clear gel is in some cases close to the value recovered in the other conditions (higher scattering) while other times is far from this value. This variability also within the

Biomedical Optics EXPRESS

same phantom can be due to parameters which are non-perfectly under control (e.g. thickness of the fluid layer) whose effect is greatly enhanced when using water-clear gel.

The deviation in the recovered spectra can be found also in the retrieved μ_s' with the water-clear gel. Indeed, Fig. 4 and Fig. 5 show that, for both SDDs, the reduced scattering is highly underestimated and the spectral decrease trend is lost. As for absorption, this effect is more evident for higher values of μ_a and μ_s'.

It has to be noted that for phantoms with high absorption/reduced scattering coefficients measured at SDD = 3 cm, the recovered spectra are not meaningful since they are dominated by noise. This is a well-known and expected behavior due to the low number of recorded photons which leads to a poor dynamic range of the measurements, thus impairing the fitting procedure.

Looking at Fig. 4 and Fig. 5, it is also possible to appreciate a slight overestimation of μ_s' for body lotion 1, which can be observed in all situations. This behavior can be attributed to the high viscosity of the fluid, which can be due to a high concentration of solid scattering particles in the fluid, thus resulting in an extremely high scattering.

All these considerations are confirmed also by Figs. 6 to 9 where the relative error in the recovered optical properties with respect to the "reference measurement" (i.e. with black velvet) are reported. It is clearly noticeable that for all fluids (except for water-clear one and body lotion 1) the error is almost negligible, provided that the recovery of the optical properties is robust enough (e.g. there is enough signal to fit the data). On the other hand, the water clear gel shows a high relative error (> 50%) in both absorption and reduced scattering coefficients, which is larger for high absorbing/diffusing phantoms. For what concerns "body lotion 1", we notice a not negligible error (ranging from 10% to 30%) in the reduced scattering coefficient, which is more evident for the less diffusive phantoms (first row of Fig. 8 and Fig. 9).

To prove that the water-clear gel allows the propagation of direct light between source and detector positions, the DTOFs for the phantoms with the lowest and highest absorption and reduced scattering coefficients (corner panels of Figs. 2-5) measured at 800 nm for the water-clear gel are reported in Fig. 10 and Fig. 11 (respectively for SDD of 2 and 3 cm), together with those obtained for the turbid gel, the body lotion 1 and the standard condition. It is evident that for the water-clear gel there is a distortion of the curve as well as an anticipation of the peak (more evident for larger value of μ_s'). All those features are compatible with the hypothesis of direct light leakage, which causes a spurious peak before the "true" diffusive one (i.e. due to photons re-emitted from the medium). Moreover, the discrepancies are more marked for phantoms with higher scattering and absorption (i.e. longer photon paths and delayed detection and stronger attenuation), thus making the direct light propagation more evident. On the other hand, as expected from results reported above, there are no significant differences between the standard condition and the turbid gel. This hypothesis is confirmed by Fig. 10 as the raw curves obtained with body lotion 1 (cyan ones) are generally characterized by lower signal as well as a broadening and shift to longer times with respect to standard situation and turbid gel.

Additionally, Fig. 11 clearly confirms that, in the absence of direct light propagation, the signal for phantoms with high absorption and reduced scattering coefficients is low, thus leading to a low signal-to-noise ratio which impairs the fitting procedure, as discussed before.

Biomedical Optics EXPRESS

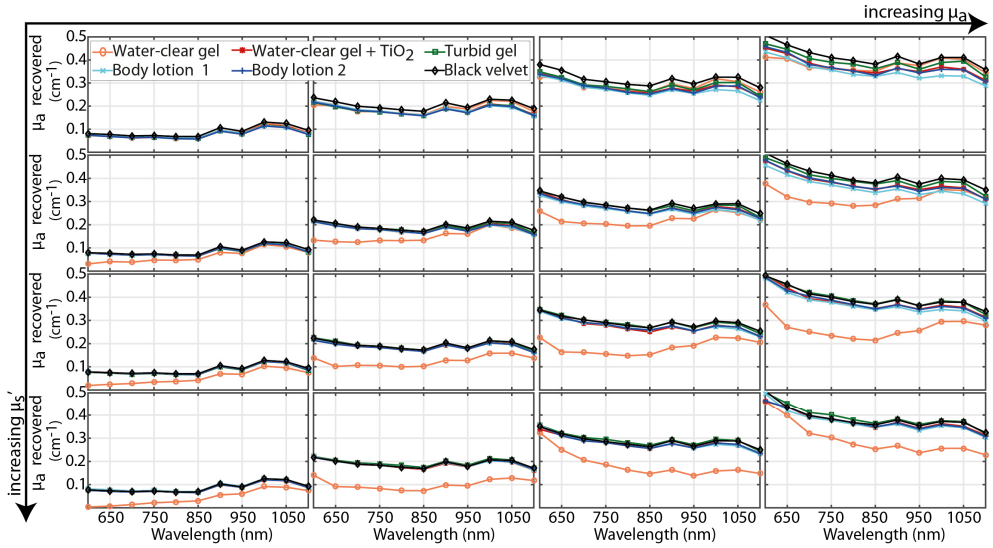

Fig. 2. Graphs of recovered absorption spectra for all the 16 phantoms at SDD = 2 cm. For each phantom, the results obtained using all 5 fluids and the black velvet (different colors, see labels) are reported.

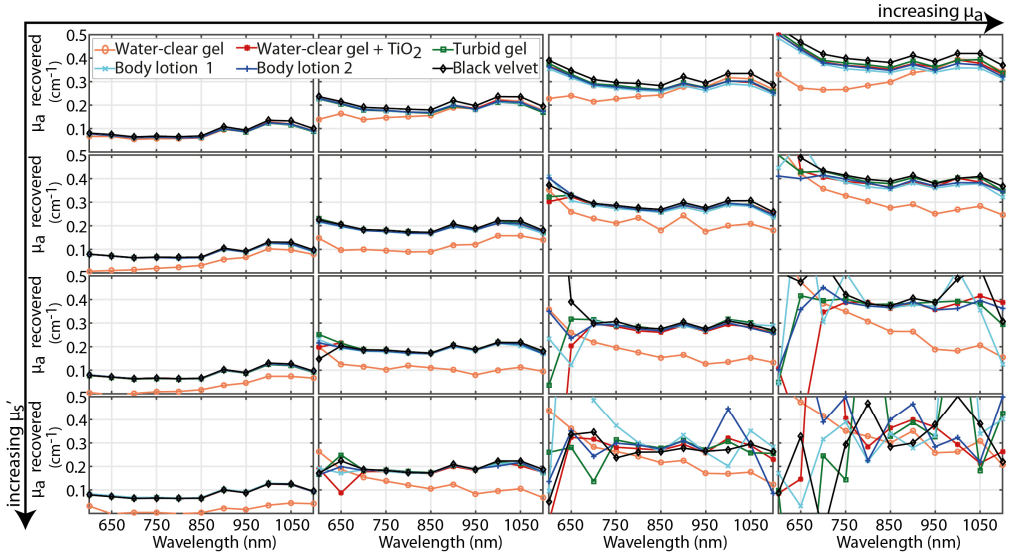

Fig. 3. Graphs of recovered absorption spectra for all 16 phantoms at SDD = 3 cm. For each phantom, the results obtained using all 5 fluids and the black velvet (different colors, see labels) are reported.

Biomedical Optics EXPRESS

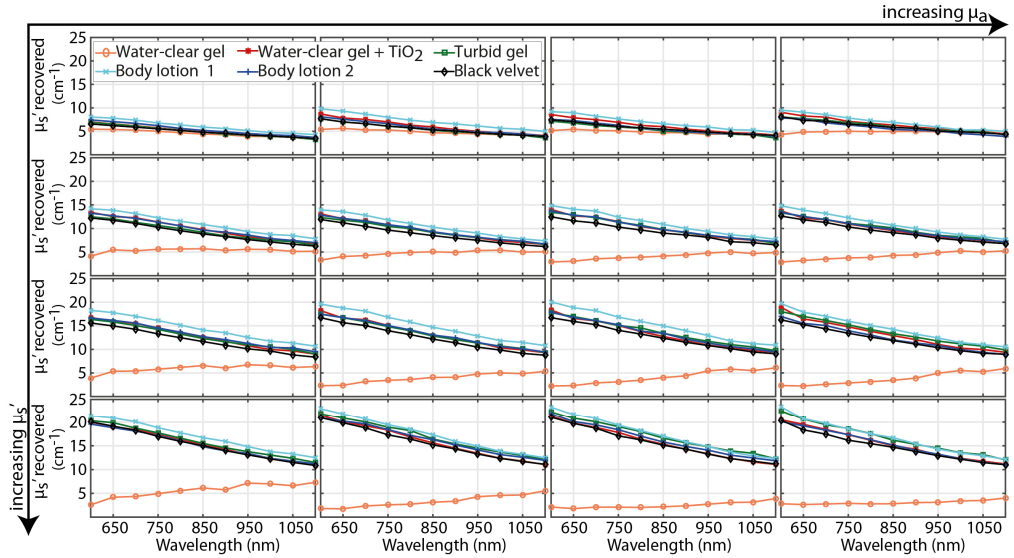

Fig. 4. Graphs of recovered reduced scattering spectra at SDD = 2 cm for all 16 phantoms. For each phantom, the results obtained using all 5 fluids and the black velvet (different colors, see labels) are reported.

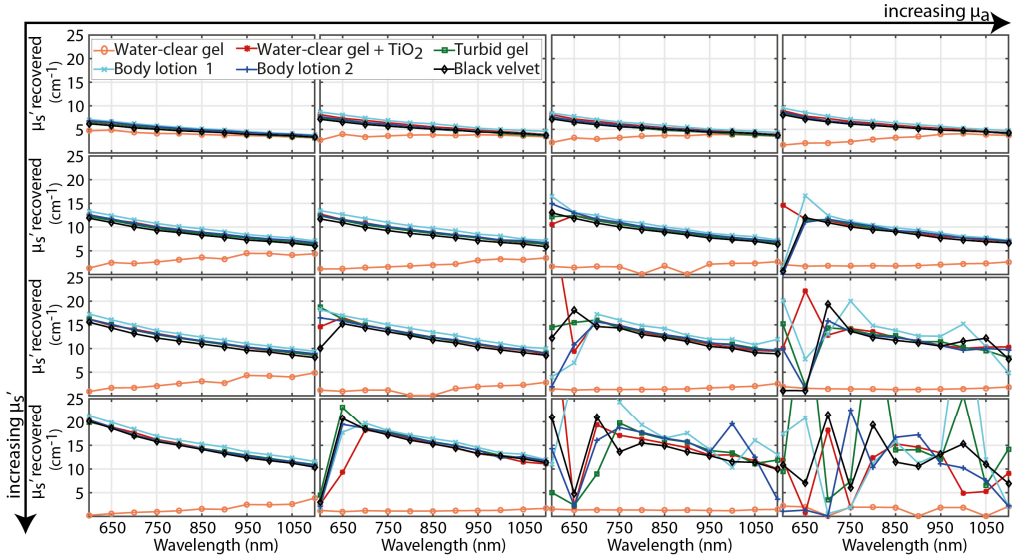

Fig. 5. Graphs of recovered reduced scattering spectra at SDD = 3 cm for all 16 phantoms. For each phantom, the results obtained using all 5 fluids and the black velvet (different colors, see labels) are reported.

Biomedical Optics EXPRESS

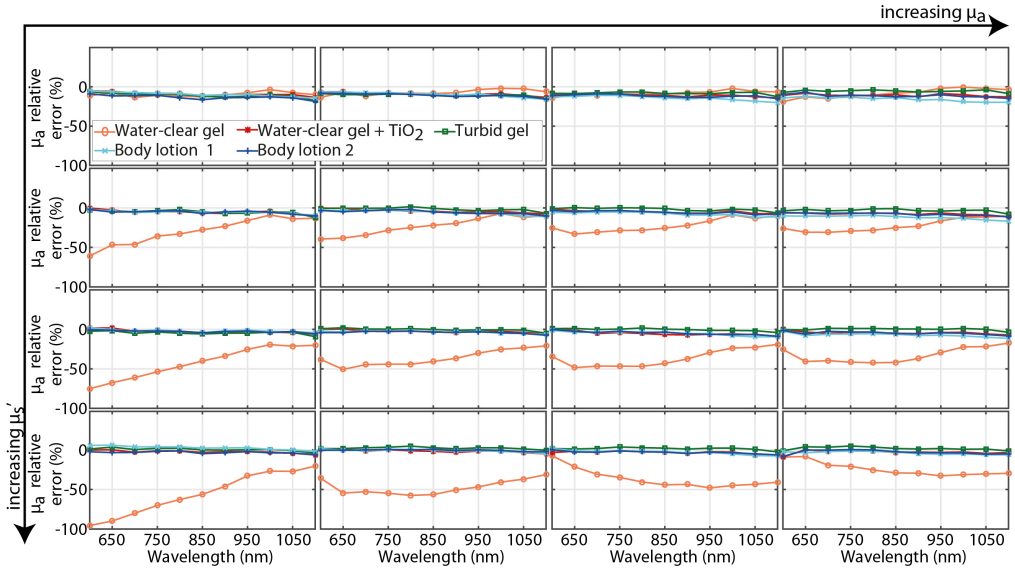

Fig. 6. Graphs of relative error in the estimate of the absorption coefficient over the whole spectrum at SDD = 2 cm for all the 16 phantoms. For each phantom, the error with respect to the black velvet is reported for all the 5 fluids.

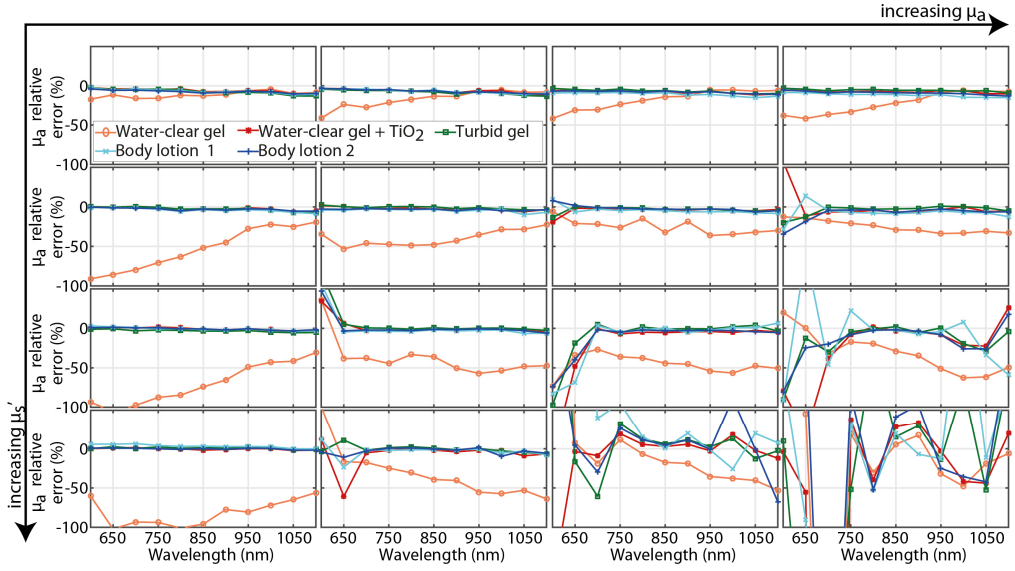

Fig. 7. Graphs of relative error in the estimate of the absorption coefficient over the whole spectrum at SDD = 3 cm for all the 16 phantoms. For each phantom, the error with respect to the black velvet is reported for all the 5 fluids.

Biomedical Optics EXPRESS

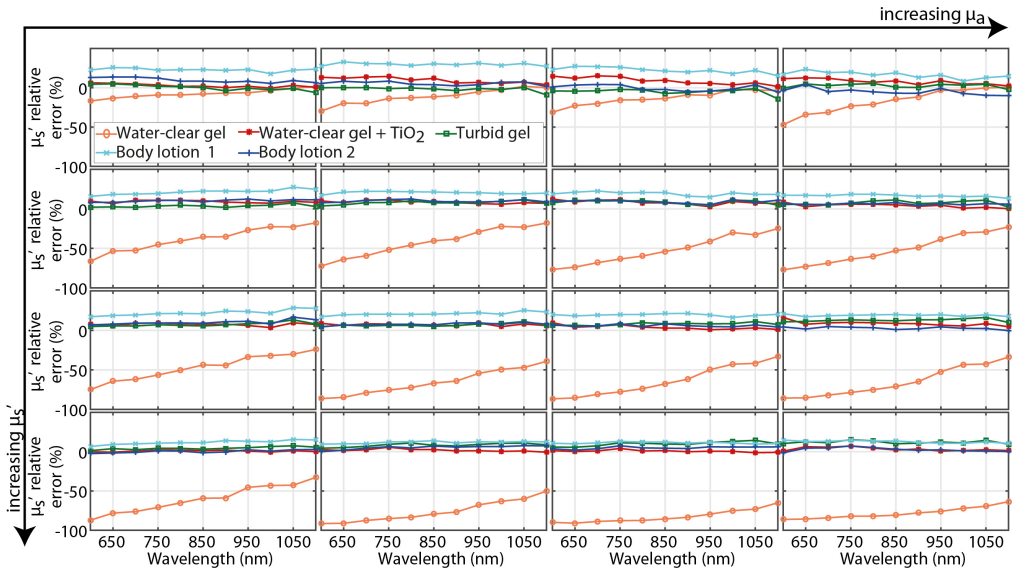

Fig. 8. Graphs of relative error in the estimate of the reduced scattering coefficient over the whole spectrum at SDD = 2 cm for all the 16 phantoms. For each phantom, the error with respect to the black velvet is reported for all the 5 fluids.

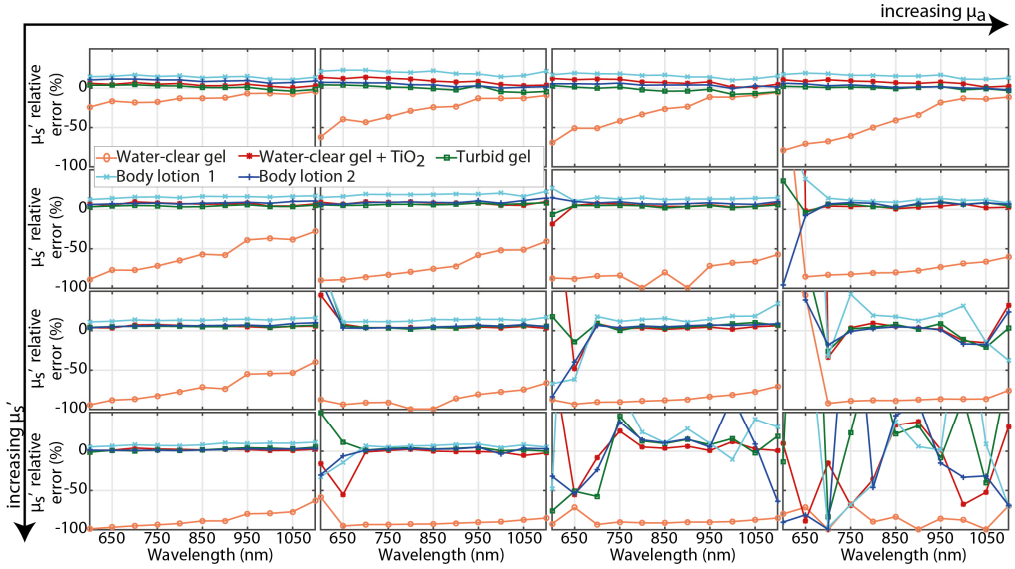

Fig. 9. Graphs of relative error in the estimate of the reduced scattering coefficient over the whole spectrum at SDD = 3 cm for all 16 the phantoms. For each phantom, the error with respect to the black velvet is reported for all 5 the fluids.

Biomedical Optics EXPRESS

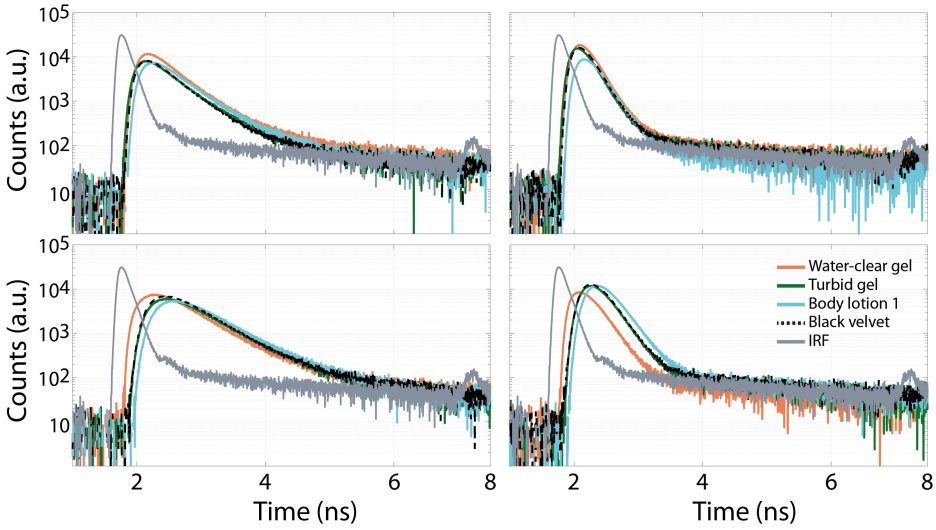

Fig. 10. Raw DTOF curves recorded at 800 nm with SDD = 2 cm, and corresponding to the outmost plots of Fig. 2 and Fig. 4 (i.e. lowest/highest scattering on first/second row and lowest/highest absorption on the first/second column) when using water-clear gel (orange line), turbid gel (green line), body lotion 1 (blue line) and black velvet (black line). To better enlighten the effect of the direct light also the IRF (gray line) is reported in each graph.

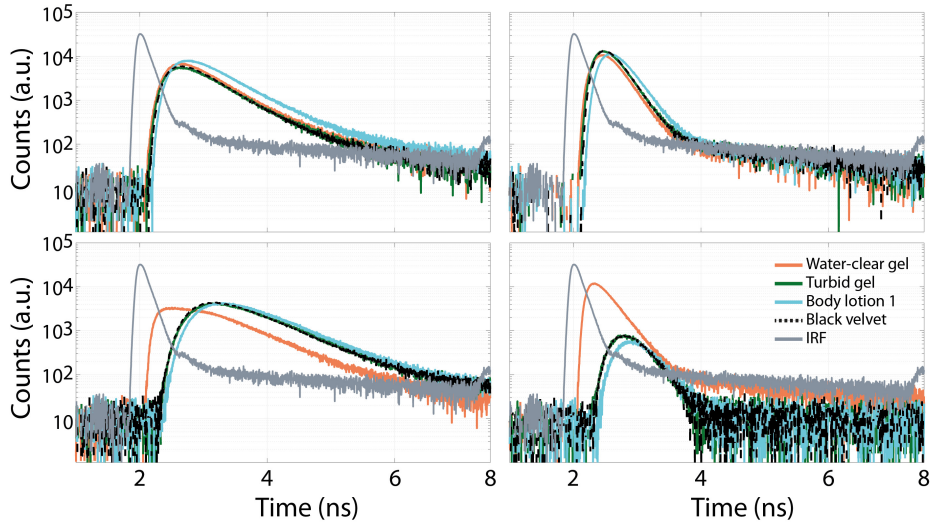

Fig. 11. Raw DTOF curves recorded at 800 nm with SDD = 3 cm, and corresponding to the outmost plots of Fig. 3 and Fig. 5 (i.e. lowest/highest scattering on first /second row and lowest/highest absorption on the first/second column) when using water-clear gel (orange line), turbid gel (green line), body lotion 1 (blue line) and black velvet (black line). To better enlighten the effect of the direct light also the IRF (gray line) is reported in each graph.

3.2 DCS measurements

We have measured the liquid phantom in the same 6 different configurations of the probe-phantom interface already tested for DOS measurements.

Figure 12 shows the average measured D_b related to the different configurations with error bars due to the acquisition noise. Figure 12 highlights that the same particle Brownian diffusion coefficient as measured with the probe covered with black velvet is retrieved, in the

Biomedical Optics EXPRESS

limit of experimental error, using all the probe-phantom interface fluids, except for the water-clear gel. This last configuration causes a 30% underestimation of the D_b, due to direct light channeling between source and detector fiber bundle tips. DCS measurements highlight that the light channeling due to the water clear gel is responsible for a higher error when determining the D_b with longer source-detector separations (where the signal in the detector due the diffused photons has a lower intensity). Additionally, a larger variability of the D_b is obtained for the body lotion 1: this may be due to higher concentration of scattering particles (as enlighten in Sect. 3.1) thus resulting in a lower signal and higher variability as reported in Table 1.

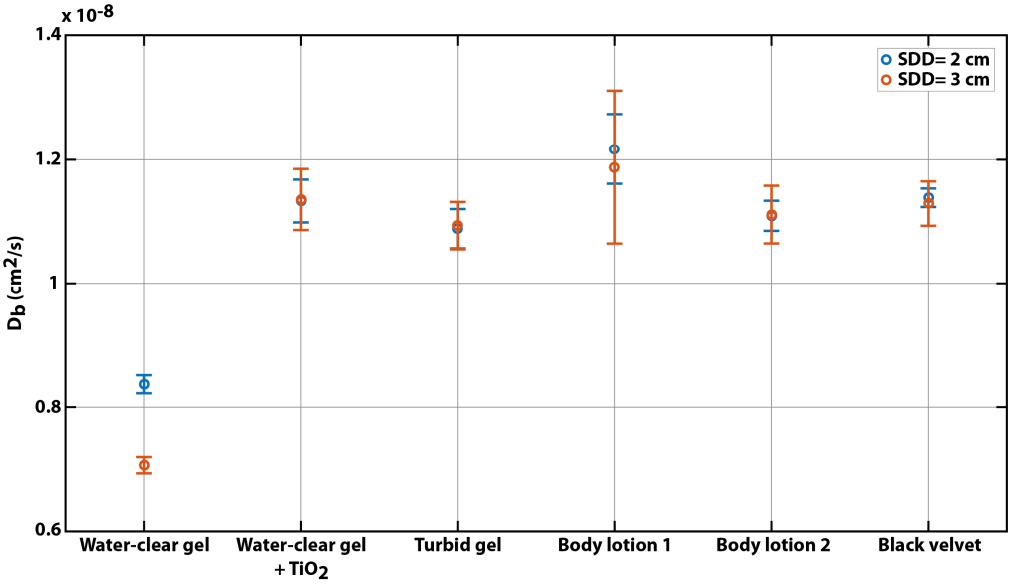

Fig. 12. Particle Brownian diffusion coefficients retrieved for the DCS phantom with the 6 different probe interface materials.

Table 1. Averages and standard deviations of the photon counts (in kcps) in DCS measurements for each experimental condition

	SDD = 2 cm		SDD = 3 cm	
Material	Average	St. Dev.	Average	St. Dev.
Water-clear gel	210.72	14.55	308.27	16.12
Water-clear gel + TiO_2	83.02	5.06	161.69	15.62
Turbid gel	91.65	4.96	183.54	8.28
Body lotion 1	48.76	5.79	98.28	0.96
Body lotion 2	87.62	6.04	174.40	8.69
Black velvet	168.82	10.07	309.83	10.54

Biomedical Optics EXPRESS

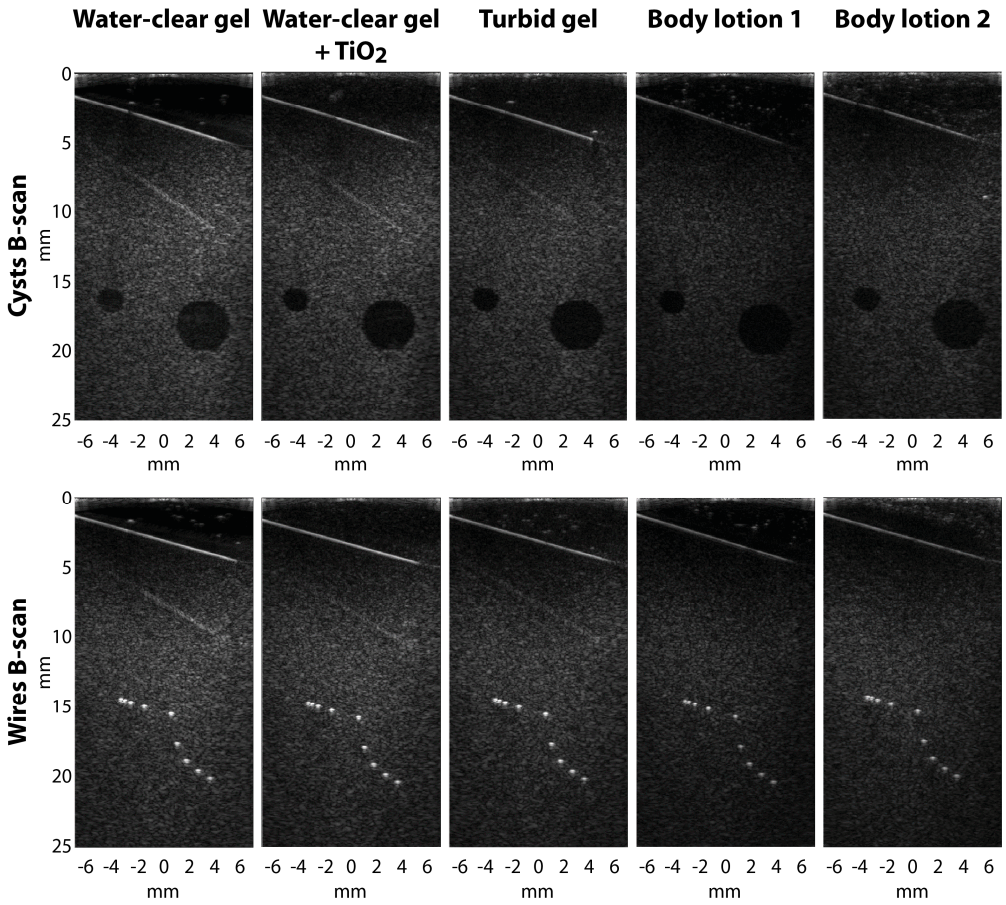

Fig. 13. US images acquired on both cysts and wires regions of the Gammex 404GS phantom (top and bottom rows respectively) with the several fluids (columns). The topmost white line corresponds to the US phantom entrance as the probe is tilted. DR = 40 dB.

3.3 Ultrasound imaging experiment

Figure 13 shows the images (cysts and wires B-scans, rows) acquired using the various fluids already tested for DOS and DCS (columns). All B-mode images are displayed with 40 dB dynamic range (DR). B-scans through commercial gels (water-clear gel and turbid gel) can be taken as reference since they exhibit, among all other fluids, the best coupling features. Indeed, good SoS matching is revealed by the well preserved circular shape of the cyst and the good wires resolution, as well as low attenuation is shown by the high overall brightness intensity in the image. Finally, the presence of the reduplication artifact of the gel/phantom interface confirms that both US attenuation and SoS in the coupling agent are well suited for acoustic coupling.

The water-clear gel with TiO_2 appears to be also an interesting candidate as spatial and contrast resolution, as well as spatial fidelity with regard to the reference images, are well preserved. Indeed, the width of the wires remains as thin as on the reference B-scan and darkness of the cyst with regard to the speckle brightness intensity is similar to the reference image thus indicating that the spatial and contrast resolution are preserved. On the other hand, body lotions are more attenuating medium, especially Body Lotion 1, but they seem to exhibit nevertheless a good SoS matching with those from soft tissue as no distortions are noticeable on either the cysts nor the wires. Indeed, a decrease in the overall brightness intensity in the

Biomedical Optics EXPRESS

image is a good indicator of the gel attenuation provided that it has effectively a good SoS matching.

4. Conclusions

In this paper, we analysed the effect of several types of possible US-coupling fluids to be used in multimodal diffuse optical and ultrasound measurements. We clearly noticed that a water-clear gel can generate a direct light propagation between source and detection, thus impairing both diffuse optical spectroscopy and diffuse correlation spectroscopy measurements. On the contrary, we proved that diffusive fluids can successfully be used to prevent direct light propagation. However, high viscosity fluids can distort optical measurements and reduce the quality of ultrasound investigation. A commercially-available turbid ultrasound gel, as well as an home-made dispersion of scattering particles into a water-clear commercially-available US gel, demonstrated the best performance in both optical and ultrasound measurements, representing for this reason the best choice as coupling materials to be used in case of multimodal optical-US investigations.

Funding

European Union's Horizon 2020 research and innovation programme (688303 (LUCA), 731877 (SOLUS) and 654148 (Laserlab-Europe)); Fundació CELLEX Barcelona, the "Severo Ochoa" Programme for Centres of Excellence in R&D (SEV-2015-0522), the Obra social "la Caixa" Foundation (LlumMedBcn).

Acknowledgments

The authors wish to acknowledge Luca Baratelli from Politecnico di Milano for his help during experimental measurements.

SOLUS and LUCA are initiatives of the Photonics Public Private Partnership.

Disclosures

ICFO has equity ownership in the spin-off company HemoPhotonics S.L. Potential financial conflicts of interest and objectivity of research have been monitored by ICFO's Knowledge & Technology Transfer Department. No financial conflicts of interest were identified.

References

1. N. Vogler, S. Heuke, T. W. Bocklitz, M. Schmitt, and J. Popp, "Multimodal Imaging Spectroscopy of Tissue," Annu. Rev. Anal. Chem. (Palo Alto, Calif.) **8**(1), 359–387 (2015).
2. D. W. Townsend, "Multimodality imaging of structure and function," Phys. Med. Biol. **53**(4), R1–R39 (2008).
3. B. J. Pichler, A. Kolb, T. Nägele, and H.-P. Schlemmer, "PET/MRI: Paving the Way for the Next Generation of Clinical Multimodality Imaging Applications," J. Nucl. Med. **51**(3), 333–336 (2010).
4. S. R. Cherry, "Multimodality Imaging: Beyond PET/CT and SPECT/CT," Semin. Nucl. Med. **39**(5), 348–353 (2009).
5. W. P. Segars, G. Sturgeon, S. Mendonca, J. Grimes, and B. M. W. Tsui, "4D XCAT phantom for multimodality imaging research," Med. Phys. **37**(9), 4902–4915 (2010).
6. X. Li, X.-N. Zhang, X.-D. Li, and J. Chang, "Multimodality imaging in nanomedicine and nanotheranostics," Cancer Biol. Med. **13**(3), 339–348 (2016).
7. L. Curiel, R. Chopra, and K. Hynynen, "Progress in multimodality imaging: Truly simultaneous ultrasound and magnetic resonance imaging," IEEE Trans. Med. Imaging **26**(12), 1740–1746 (2007).
8. A. Yodh and B. Chance, "Spectroscopy and imaging with diffusing light," Phys. Today **48**(3), 34–40 (1995).
9. A. Pifferi, A. Farina, A. Torricelli, G. Quarto, R. Cubeddu, and P. Taroni, "Review: Time-domain broadband near infrared spectroscopy of the female breast: A focused review from basic principles to future perspectives," J. Near Infrared Spectrosc. **20**(1), 223–235 (2012).
10. T. Durduran, R. Choe, W. B. Baker, and A. G. Yodh, "Diffuse optics for tissue monitoring and tomography," Rep. Prog. Phys. **73**(7), 076701 (2010).
11. A. Puszka, L. Di Sieno, A. Dalla Mora, A. Pifferi, D. Contini, A. Planat-Chrétien, A. Koenig, G. Boso, A. Tosi, L. Hervé, and J.-M. Dinten, "Spatial resolution in depth for time-resolved diffuse optical tomography using short source-detector separations," Biomed. Opt. Express **6**(1), 1–10 (2015).
12. "SOLUS project," http://www.solus-project.eu/.

Biomedical Optics EXPRESS

13. "LUCA project," http://www.luca-project.eu.
14. H. Vavadi, A. Mostafa, F. Zhou, K. M. S. Uddin, M. Althobaiti, C. Xu, R. Bansal, F. Ademuyiwa, S. Poplack, and Q. Zhu, "Compact ultrasound-guided diffuse optical tomography system for breast cancer imaging," J. Biomed. Opt. **24**(2), 1–9 (2018).
15. C. Xu, H. Vavadi, A. Merkulov, H. Li, M. Erfanzadeh, A. Mostafa, Y. Gong, H. Salehi, S. Tannenbaum, and Q. Zhu, "Ultrasound-Guided Diffuse Optical Tomography for Predicting and Monitoring Neoadjuvant Chemotherapy of Breast Cancers: Recent Progress," Ultrason. Imaging **38**(1), 5–18 (2016).
16. F. Zhou, A. Mostafa, and Q. Zhu, "Improving breast cancer diagnosis by reducing chest wall effect in diffuse optical tomography," J. Biomed. Opt. **22**(3), 036004 (2017).
17. Q. Zhu, "Optical tomography with ultrasound localization: Initial clinical results and technical challenges," Technol. Cancer Res. Treat. **4**(3), 235–244 (2005).
18. V. C. Kavuri and H. Liu, "Hierarchical clustering method to improve transrectal ultrasound-guided diffuse optical tomography for prostate cancer imaging," Acad. Radiol. **21**(2), 250–262 (2014).
19. A. H. Bamett, J. P. Culver, A. G. Sorensen, A. Dale, and D. A. Boas, "Robust inference of baseline optical properties of the human head with three-dimensional segmentation from magnetic resonance imaging," Appl. Opt. **42**(16), 3095–3108 (2003).
20. P. K. Yalavarthy, B. W. Pogue, H. Dehghani, C. M. Carpenter, S. Jiang, K. D. Paulsen, Q. Zhang, T. J. Brukilacchio, A. Li, J. J. Stott, T. Chaves, E. Hillman, T. Wu, M. Chorlton, E. Rafferty, R. H. Moore, D. B. Kopans, A. Li, G. Boverman, Y. Zhang, D. Brooks, E. L. Miller, M. E. Kilmer, Q. Zhang, E. M. C. Hillman,11 R. L. Barbour, H. L. Graber, J. W. Chang, S. L. S. Barbour, P. C. Koo, R. Aronson, W. Pogue, S. Jiang, H. Dehghani, S. Srinivasan, C. Kogel, T. D. Tosteson, J. Weaver, S. P. Poplack, K. D. Paulsen, K. D. Paulsen, H. Jiang, T. O. Mcbride, B. W. Pogue, and U. L. Osterberg, "Structural information within regularization matrices improves near infrared diffuse optical tomography," Opt. Express **15**, 8043–8058 (2007).
21. L. Zhang, Y. Zhao, S. Jiang, B. W. Pogue, and K. D. Paulsen, "Direct regularization from co-registered anatomical images for MRI-guided near-infrared spectral tomographic image reconstruction," Biomed. Opt. Express **6**(9), 3618–3630 (2015).
22. V. Ntziachristos, X. H. Ma, and B. Chance, "Time-correlated single photon counting imager for simultaneous magnetic resonance and near-infrared mammography," Rev. Sci. Instrum. **69**(12), 4221–4233 (1998).
23. V. Ntziachristos, A. G. Yodh, M. D. Schnall, and B. Chance, "MRI-guided diffuse optical spectroscopy of malignant and benign breast lesions," Neoplasia **4**(4), 347–354 (2002).
24. S. Srinivasan, C. M. Carpenter, H. R. Ghadyani, S. J. Taka, P. A. Kaufman, R. M. Diflorio-Alexander, W. A. Wells, B. W. Pogue, and K. D. Paulsen, "Image guided near-infrared spectroscopy of breast tissue in vivo using boundary element method," J. Biomed. Opt. **15**(6), 061703 (2010).
25. C. M. Carpenter, B. W. Pogue, S. Jiang, J. Wang, B. A. Hargreaves, R. Rakow-Penner, B. L. Daniel, and K. D. Paulsen, "MR water quantitative priors improves the accuracy of optical breast imaging," IEEE Trans. Med. Imaging **30**(1), 159–168 (2011).
26. S. Fantini, B. Frederick, and A. Sassaroli, "Perspective: Prospects of non-invasive sensing of the human brain with diffuse optical imaging," APL Photonics **3**(11), 110901 (2018).
27. V. Quaresima and M. Ferrari, "Functional Near-Infrared Spectroscopy (fNIRS) for Assessing Cerebral Cortex Function During Human Behavior in Natural/Social Situations: A Concise Review," Organ. Res. Methods **22**(1), 46–68 (2019).
28. N. A. Carbone, D. I. Iriarte, and J. A. Pomarico, "Wide field continuous wave reflectance optical topography including a clear layer on top of the diffusive surface," J. Near Infrared Spectrosc. **25**(3), 165–171 (2017).
29. S. Del Bianco, F. Martelli, F. Cignini, G. Zaccanti, A. Pifferi, A. Torricelli, A. Bassi, P. Taroni, and R. Cubeddu, "Liquid phantom for investigating light propagation through layered diffusive media," Opt. Express **12**(10), 2102–2111 (2004).
30. S. Konugolu Venkata Sekar, A. Dalla Mora, I. Bargigia, E. Martinenghi, C. Lindner, P. Farzam, M. Pagliazzi, T. Durduran, P. Taroni, A. Pifferi, and A. Farina, "Broadband (600-1350 nm) Time-Resolved Diffuse Optical Spectrometer for Clinical Use," IEEE J. Sel. Top. Quantum Electron. **22**(3), 7100609 (2016).
31. E. Martinenghi, L. Di Sieno, D. Contini, M. Sanzaro, A. Pifferi, and A. Dalla Mora, "Time-resolved single-photon detection module based on silicon photomultiplier: A novel building block for time-correlated measurement systems," Rev. Sci. Instrum. **87**(7), 073101 (2016).
32. H. Wabnitz, A. Jelzow, M. Mazurenka, O. Steinkellner, R. Macdonald, D. Milej, N. Żołek, M. Kacprzak, P. Sawosz, R. Maniewski, A. Liebert, S. Magazov, J. Hebden, F. Martelli, P. Di Ninni, G. Zaccanti, A. Torricelli, D. Contini, R. Re, L. Zucchelli, L. Spinelli, R. Cubeddu, and A. Pifferi, "Performance assessment of time-domain optical brain imagers, part 2: nEUROPt protocol," J. Biomed. Opt. **19**(8), 086012 (2014).
33. A. Pifferi, A. Torricelli, A. Bassi, P. Taroni, R. Cubeddu, H. Wabnitz, D. Grosenick, M. Möller, R. Macdonald, J. Swartling, T. Svensson, S. Andersson-Engels, R. L. P. van Veen, H. J. C. M. Sterenborg, J.-M. Tualle, H. L. Nghiem, S. Avrillier, M. Whelan, and H. Stamm, "Performance assessment of photon migration instruments: the MEDPHOT protocol," Appl. Opt. **44**(11), 2104–2114 (2005).
34. D. Contini, A. Torricelli, A. Pifferi, L. Spinelli, F. Paglia, and R. Cubeddu, "Multi-channel time-resolved system for functional near infrared spectroscopy," Opt. Express **14**(12), 5418–5432 (2006).
35. L. Di Sieno, A. Dalla Mora, G. Boso, A. Tosi, A. Pifferi, R. Cubeddu, and D. Contini, "Diffuse optics using a dual window fast-gated counter," Appl. Opt. **53**(31), 7394–7401 (2014).
36. A. Dalla Mora, E. Martinenghi, D. Contini, A. Tosi, G. Boso, T. Durduran, S. Arridge, F. Martelli, A. Farina, A.

Biomedical Optics EXPRESS

Torricelli, and A. Pifferi, "Fast silicon photomultiplier improves signal harvesting and reduces complexity in time-domain diffuse optics," Opt. Express **23**(11), 13937–13946 (2015).
37. L. Di Sieno, J. Nissinen, L. Hallman, E. Martinenghi, D. Contini, A. Pifferi, J. Kostamovaara, and A. Dalla Mora, "Miniaturized pulsed laser source for time-domain diffuse optics routes to wearable devices," J. Biomed. Opt. **22**(8), 1–9 (2017).
38. R. Re, E. Martinenghi, A. Dalla Mora, D. Contini, A. Pifferi, and A. Torricelli, "Probe-hosted silicon photomultipliers for time-domain functional near-infrared spectroscopy: phantom and in vivo tests," Neurophotonics **3**(4), 045004 (2016).
39. M. Buttafava, E. Martinenghi, D. Tamborini, D. Contini, A. Dalla Mora, M. Renna, A. Torricelli, A. Pifferi, F. Zappa, and A. Tosi, "A Compact Two-Wavelength Time-Domain NIRS System Based on SiPM and Pulsed Diode Lasers," IEEE Photonics J. **9**(1), 1–14 (2017).
40. H. Wabnitz, D. R. Taubert, M. Mazurenka, O. Steinkellner, A. Jelzow, R. Macdonald, D. Milej, P. Sawosz, M. Kacprzak, A. Liebert, R. Cooper, J. Hebden, A. Pifferi, A. Farina, I. Bargigia, D. Contini, M. Caffini, L. Zucchelli, L. Spinelli, R. Cubeddu, and A. Torricelli, "Performance assessment of time-domain optical brain imagers, part 1: basic instrumental performance protocol," J. Biomed. Opt. **19**(8), 086010 (2014).
41. D. Contini, F. Martelli, and G. Zaccanti, "Photon migration through a turbid slab described by a model based on diffusion approximation. I. Theory," Appl. Opt. **36**(19), 4587–4599 (1997).
42. L. Cortese, G. L. Presti, M. Pagliazzi, D. Contini, A. Dalla Mora, A. Pifferi, S. K. V. Sekar, L. Spinelli, P. Taroni, M. Zanoletti, U. M. Weigel, S. de Fraguier, A. Nguyen-Dihn, B. Rosinski, and T. Durduran, "Liquid phantoms for near-infrared and diffuse correlation spectroscopies with tunable optical and dynamic properties," Biomed. Opt. Express **9**(5), 2068–2080 (2018).